HOKKAIDO UNIVERSITY

Title	Aging of Passive Oxide on SUS304 Stainless Steel in a Sulfuric Acid Solution
Author(s)	Ohtsuka, Toshiaki; Ueda, Mikito; Abe, Masatoshi
Citation	J. Electrochemical Society, 163(8), C459-C469 https://doi.org/10.1149/2.0721608jes
Issue Date	2016
Doc URL	https://hdl.handle.net/2115/62190
Rights	© The Electrochemical Society, Inc. 2016. All rights reserved. Except as provided under U.S. copyright law, this work may not be reproduced, resold, distributed, or modified without the express permission of The Electrochemical Society (ECS). The archival version of this work was published in J. Electrochem. Soc. 2016 volume 163, issue 8, C459-C469 .
Rights(URL)	https://creativecommons.org/licenses/by-nc-nd/4.0/
Type	journal article
File Information	J. Electrochem. Soc.-2016-Ohtsuka-C459-69.pdf

Hokkaido University Collection of Scholarly and Academic Papers : HUSCAP

Aging of Passive Oxide on SUS304 Stainless Steel in a Sulfuric Acid Solution

Toshiaki Ohtsuka,[z] Mikito Ueda,[*] and Masatoshi Abe[a]

Division of Materials Science and Engineering, Faculty of Engineering, Hokkaido University, Sapporo, Hokkaido 060-8628, Japan

The passive oxide film on SUS 304 stainless steel (SS) was studied in a 0.1 mol dm^{-3} sulfuric acid solution as a function of passivation time. The passive oxide films were measured by ellipsometry and X-ray photoelectron spectroscopy (XPS). A Mott-Schottky plot of the film capacitance was employed to determine the donor density in the n-type semiconducting oxide film, and current measurements of the Fe^{3+}/Fe^{2+} redox couple were employed to investigate the electronic transfer process on the passive oxide film. The passive oxide consists of Cr-Fe-Ni oxides in which enrichment of Cr to 57 mol% occurs as the potential increases. During the aging of the passive oxide at 0.6 V vs. Ag/AgCl/saturated KCl (SSC) for 43 ks, the current decreased from 30 $\mu A\ cm^{-2}$ at 10 s to 0.025 $\mu A\ cm^{-2}$ at 43 ks, and the Cr ratio in the oxide increased from 49 to 57 mol% with an increase in the O^{2-} ratio. Notably, the film thickness remained nearly constant at 1.3 nm during the aging process. Enrichment of the Cr content resulted in a decrease in the donor density of the n-type semiconducting passive oxide and the inhibition of electronic charge transfer from/to the Fe^{3+}/Fe^{2+} redox couple in the electrolyte.

© The Author(s) 2016. Published by ECS. This is an open access article distributed under the terms of the Creative Commons Attribution Non-Commercial No Derivatives 4.0 License (CC BY-NC-ND, http://creativecommons.org/licenses/by-nc-nd/4.0/), which permits non-commercial reuse, distribution, and reproduction in any medium, provided the original work is not changed in any way and is properly cited. For permission for commercial reuse, please email: oa@electrochem.org. [DOI: 10.1149/2.0721608jes] All rights reserved.

Manuscript submitted December 2, 2015; revised manuscript received May 16, 2016. Published June 2, 2016.

The corrosion resistance of stainless steel is the result of surface passive films enriched in chromium. The passive oxide film on conventional austenitic stainless steel (SS) SUS304 has been investigated with a focus on its composition,[1–6] thickness[7–9] and semiconducting properties.[5,6,10–20] For the oxide formed in an acidic aqueous solution, the chromium oxide component was enriched to a ratio of approximately 50–60 mol % in passive oxide in an acidic aqueous solution.[1–3] Its thickness was estimated by ellipsometry to be 1–2 nm.[8,20] In neutral and slightly alkaline solutions, the passive oxide consists of an inner chromium-rich oxide layer and an outer iron-rich oxide layer.[4–6] The semiconducting properties of passive oxides[5,6,10–20] has been estimated from a Mott-Schottky plot of the capacitance data and photoelectrochemical measurements. The Mott-Schottky plot in the potential range, in which little reduction of the film occurs, indicated that the passive oxide had an n-type semiconducting property.[6,10,13,16,19,21] However, the results of photo-electrochemical measurement indicated that the passive oxide had both n-type and p-type semiconducting properties.[5,17,18]

Because there are no in situ techniques available to determine the composition of the thin passive oxide on 304 SS, ex-situ spectroscopies performed in vacuum, such as X-ray photoelectron spectroscopy (XPS)[1–4,6] and Auger electron spectroscopy (AES),[4,5] have been used to obtain this information. Additionally, the film composition and structure were determined using simulations involving photoelectron signals and the attenuation of these signals of the ionic and metallic species. For the anodic passive oxide on 304 SS and on Fe-Cr alloys in sulfuric acid solutions, quantitative simulation was reported by various authors by using XPS[3,21,23–26] and AES.[22] Asami et al.[21] and Kirchheim et al.[23] reported a relation between the compositions of the oxide film and the substrate of Fe-Cr alloys at various Cr concentrations. They found that enrichment of Cr in the passive oxide in a sulfuric acid solution, for example, enriched Cr in the passive oxide film to approximately 60 mol% on Fe-18 mol% Cr alloy. In addition, Marcus et al. reported the enrichment of Cr in the passive oxide on Fe-22Cr,[25,26] Fe-17Cr,[27] and Fe-18Cr-13Ni,[3] and an additional enrichment of Cr on the Fe-Cr alloy surface underneath the passive oxide.[24,25] The enrichment of Cr in the passive oxide film has been explained by selective dissolution of Fe in the acidic solution.[24,26] In connection with the Cr enrichment in the oxide film, the critical Cr ratio of the substrate to induce passivation in acidic solution has been elucidated by graph theory[27,28] and a percolation model.[29]

Previously, we reported the thickness and semiconducting properties of the passive oxide film on SUS304 SS in a 0.1 mol dm^{-3} (M) sulfuric acid solution using ellipsometry, potential modulation reflectance (PMR), and capacitance measurements.[20] The thickness of the film was in the range of 1–1.3 nm and increased as the potential increased in the passive region. In addition, a further increase in the transpassive region to 1.8 nm at 0.9 V vs. Ag/ AgCl/ saturated KCl (SSC) was observed. From the PMR results, the optical absorption edge (i.e., the bandgap energy) was found to be approximately 2.4 eV, and from the Mott-Schottky plot of the capacitance estimated by AC impedance, the donor density of the n-type semiconducting passive oxide was found to be approximately $8 \times 10^{20}\ cm^{-3}$.

In this study, we measured the Cr enrichment of the passive oxide on SUS 304 SS using XPS as a function of the potential and time period under constant potential oxidation. Additionally, the film thickness and semiconducting properties were measured as a function of time using ellipsometry and measurements of the capacitance and Fe^{3+}/Fe^{2+} reduction-oxidation (redox) current, respectively. During the aging of the passive oxide, Kirchheim et al. measured the Cr enrichment in the passive oxide on Fe-18Cr alloy in a 0.5 M H_2SO_4 solution by XPS and found a gradual enrichment of Cr from 45 mol% at 20 s to 67 mol% at 2×10^4 s at constant potential in the passive region.[24] In the present study, we also observed a gradual enrichment of Cr in the oxide film on SUS304 SS under constant potential control. Further, we compared the enrichment of Cr with the change in thickness and semiconducting properties of the oxide film during its aging.

Experimental

The composition of SUS304 stainless steel (SS) used in this study was 18.29 wt% Cr and 8.75 wt% Ni with minor components consisting of 0.066 wt% C, 0.58 wt% Si, 0.029 wt% P, 0.002 wt% S, 0.82 wt% Mn, and 0.14 wt% Mo. The SS sheet was purchased from the Japan Stainless Steel Association. The 2-mm-thick SS sheet was cut into discs with a 15-mm diameter for the electrochemical and XPS measurements and a 24-mm diameter for ellipsometry. One side of the disc was polished by an alumina abrasive with a 0.05-μm diameter to produce a mirror-like surface. The disc was fixed by a Teflon spacer or a rubber O-ring into an electrode holder made of Teflon.

*Electrochemical Society Member.
[a]Present address: Research & Development Center, Nippon Steel & Sumikin Stainless Steel Corp., Hikari, Yamaguchi 743-8550, Japan.
[z]E-mail: ohtsuka@eng.hokudai.ac.jp

Downloaded on 2016-06-13 to IP 133.87.145.210 address. Redistribution subject to ECS terms of use (see ecsdl.org/site/terms_use) unless CC License in place (see abstract).

The polished side was exposed to an electrolyte solution for the electrochemical measurements. The exposure area was 0.785 cm^2 for the electrochemical and XPS measurements and 1.130 cm^2 for the ellipsometry measurements. The other side of the disc was connected to a brass disc in the Teflon holder and then to a potentiostat using a copper lead.

The Hokuto Denko HZ-5000 and H-500 potentiostats were used for the electrochemical control. A glass cell with a 100 mL solution volume was used for the electrochemical measurements. A platinum sheet was used as a counter electrode and the reference electrode was Ag/ AgCl/ saturated KCl (SSC) on a Luggin glass capillary. The 304 SS electrode was first reduced at –0.40 V vs. SSC for 1.8 ks in a 0.1 mol dm^{-3} (M) H_2SO_4 aqueous solution to remove air-formed oxide film on the polished surface. It was then passivated under potentiostatic control in a 0.1 M H_2SO_4 solution. The redox current of Fe^{3+}/Fe^{2+} on the passivated 304 SS was measured in an acidic solution consisting of 0.1 M H_2SO_4 containing 0.05 M $(NH_4)_2Fe(SO_4)_2$ and 0.05 M $NH_4Fe(SO_4)_2$. The electrolyte was deaerated by bubbling pure N_2 gas prior to use and the electrochemical measurement was performed under pure N_2 gas passing through the electrochemical cell. All of the solutions were prepared using Milli-Q pure water and analytical grade reagents.

The AC impedance of the passivated SS was measured by a frequency response analyzer (NF Design Circuit 5020) connected to a potentiostat constructed in our laboratory. For the AC impedance, the AC amplitude at 0.01 V_{rms} was superimposed on the DC potential of the potentiostat.

To estimate the composition of the passive oxide on 304 SS, X-ray photoelectron spectroscopy (XPS) was employed using a JEOL JPS-9200. After passivation in a 0.1 M H_2SO_4 solution, the SS disc was removed from the Teflon holder, washed with pure water in the atmosphere, dried by N_2 gas, and stored in a dry box filled with N_2 gas. The SS disc was then removed from the dry box and quickly inserted into the XPS apparatus. The XPS measurement employed a MgKα X-ray source at 1253.6 eV. The calibration of the binding energy of the photoelectron was performed using the Au4f7/2 signal with a binding energy of 84.00 eV. To check the reproducibility of the XPS measurement, we measured the passive oxides formed at 0.6 V vs. SSC for 3.6 ks three times. We could estimated the cationic composition in molar ratio in the oxide, for example, X(Cr) = 0.58 ± 0.03.

The film thickness was measured by in-situ ellipsometry using a rotating analyzer automated ellipsometer with an optical arrangement that consisted of a polarizer (P)-reflection sample (S)-rotating analyzer (A). Light from an output-stabilized He-Ne laser at a wavelength of 632.8 nm was used for the measurement, and the incidence angle to the reflected electrode was $\phi_1 = 60.0$ deg. For the P-S-A arrangement, the ellipsometry parameters (i.e., tan Ψ (relative amplitude ratio of p-polarized light to s-polarized light) and Δ (relative phase retardation between p- and s-polarized light)) were estimated from the in-phase component (α) and out-of-phase component (β) of the reflected light intensity relative to two times the azimuth of the rotating analyzer (A).

$$R = R_{DC}\{1 + \alpha \cos(2A) + \beta \sin(2A)\} \quad [1]$$

$$\tan\psi \exp j\Delta = \tan P[(1+\alpha)/\{\beta \pm j(1-\alpha^2-\beta^2)^{1/2}\}] \quad [2]$$

where R_{DC} is a DC component of the reflectance and P is the fixed azimuth of the polarizer. The α and β values were measured using a two-phase lock-in amplifier. The ellipsometer was constructed in our laboratory. The α, β and R_{DC} data were typically stored in 1-s intervals in a data logger with the electrochemical data (i.e., potential and current). Ψ, Δ and the reflectance change ($\Delta R/R_0$) were calculated from the stored values using a computer program. The reflectance change was defined as:

$$\Delta R/R_0 = [R_{DC}(f) - R_{DC}(0)]/R_{DC}(0) \quad [3]$$

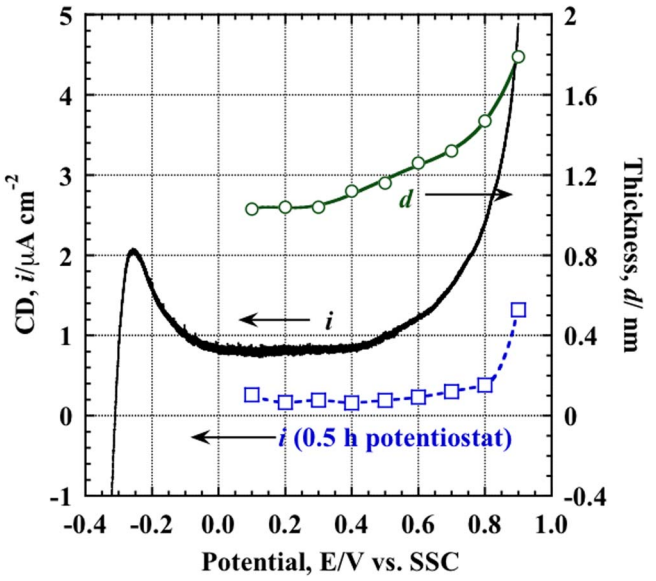

Figure 1. Potential-current curve of SUS304 SS during a potential sweep from –0.4 V vs. SSC to 0.9 V at a sweep rate of 3×10^{-4} V s^{-1} in a 0.1 M H_2SO_4 solution and during a stepwise potential increase with a step of 0.1 V and an interval of 0.5 h (–□–). The resulting potential-thickness relationship was measured during the stepwise potential increase (–○–).[21]

where $R_{DC}(f)$ is the DC reflectance of the SS surface covered by the passive oxide and $R_{DC}(0)$ is the DC reflectance of the reduced SS surface at –0.4 V.

Results

Current-potential relationship.—The potentiodynamic polarization curve for 304 SS in a 0.1 M H_2SO_4 solution is shown in Fig. 1. The measurement was performed from –0.35 V vs. SSC to 0.9 V at a potential sweep rate of 3×10^{-4} V s^{-1} after cathodic reduction at –0.4 V for 1.8 ks. A small anodic peak appeared at –0.26 V, and then the passive region in which the CD was constant at 0.8 μA cm^{-2} began at 0.0 V. The CD gradually increased at potentials higher than 0.45 V. In Fig. 1, the thickness and CD are also plotted, which reported in a previous paper.[21] The thickness was measured by a step-wise increase in the potential in the passive region with a step interval of 30 min using ellipsometry, and the CD was recorded at 30 min intervals at the individual potentials. The CD increased from 0.45 V on the potentiodynamic polarization curve; however, the CD on the potentiostatic polarization curve began to increase at 0.85 V. The transpassive dissolution of CrO_4^{2-} is assumed to begin at the potential of 0.85 V[20,23] and the passive region is in the range from –0.5 V to 0.8 V.[20,23]

Composition of the passive oxide using XPS as a function of potential.—The composition of the passive oxide formed at various potentials was estimated using XPS. Figure 2 shows examples of the XPS spectra of Fe2p3/2, Cr2p3/2, Ni2p3/2, and O1s of the reduced SS at –0.4 V for 1.8 ks and the passivated SS at potential ranging from –0.1 V to 1.1 V for 3.6 ks. The reduced surface at –0.4 V was covered by an air-formed oxide film caused by exposure to the atmosphere following reduction. On the spectra in Fig. 2, the background was compensated by a linear function. The photoelectrons were collected in the direction normal to the specimen surface. The dashed lines in Figs. 2A, 2B, and 2C indicate the peak positions of the metallic elements (i.e., Fe, Cr, and Ni). The peak positions of the metal cations in the passive oxide are located at higher binding energies. The O1s spectra shown in Fig. 2D can be deconvoluted into three peaks, which correspond to oxygen ions in O^{2-}, OH^-, and H_2O.

The 2p3/2 spectra of the three metals can be deconvoluted into metallic elements in the substrate and cationic elements in the oxide.

Downloaded on 2016-06-13 to IP 133.87.145.210 address. Redistribution subject to ECS terms of use (see ecsdl.org/site/terms_use) unless CC License in place (see abstract).

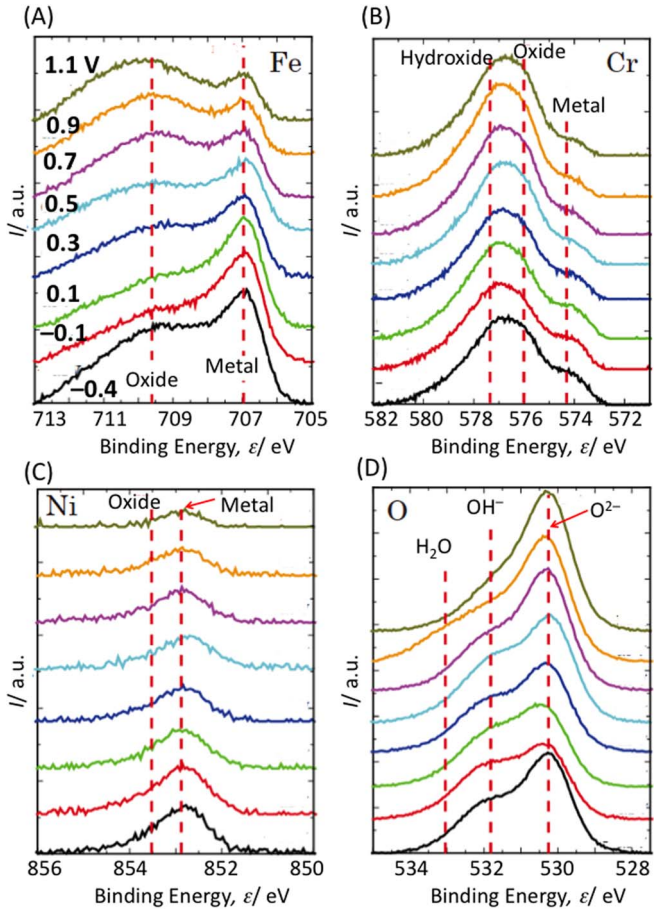

Figure 2. XPS spectra of (A) Fe2p3/2, (B) Cr2p3/2, (C) Ni2p3/2, and (D) O1s of the reduced and passivated type 304 SS at various potentials for 1 h in a 0.1 M H_2SO_4 solution. The spectra were plotted from the bottom at –0.4 V, –0.1 V, 0.1 V, 0.3 V, 0.5 V, 0.7 V, 0.9 V, and 1.1 V vs. SSC.

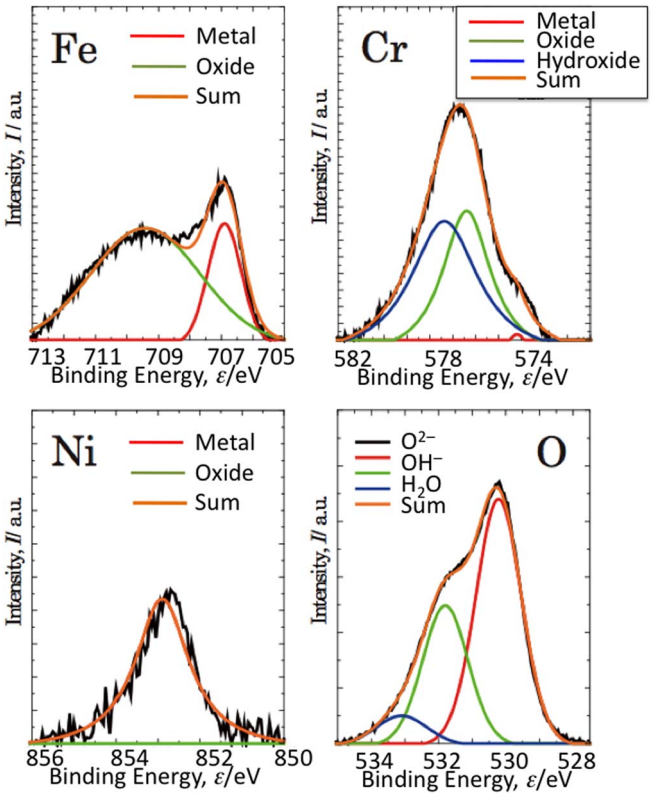

Figure 3. Examples of the deconvolution of the spectra of Fe, Cr, and Ni to oxide and metallic components and of the spectrum of O to O^{2-}, OH^-, and H_2O. The data correspond to the spectra of passivated SS at 0.1 V for 1 h.

Typical examples of the deconvolution of the spectra are shown in Fig. 3, in which the data refer to the spectra passivated at 0.6 V for 1 h. For the deconvolution of the signals of Fe, Cr, and Ni, we optimized the peak positions, P_{BE} of the metallic elements, and metal ions in the oxide with the assumption of constant *FWHM* (full width at half maximum). Likewise, the oxygen signal was deconvoluted in similar manner to the metal signals by optimizing the peak energies with constant values of *FWHM*. The data used for the deconvolution are shown in Table I. The values for the metallic elements were obtained by the XPS measurement of 304 SS after 30 min Ar^+ sputtering of the polished surface. The energy peaks of the metallic elements agree with those in the literature in a 0.1 eV range.[24,31,34,35] For the oxide elements, we assumed a single chemical state for Fe and Ni and two Cr states (i.e., Cr_2O_3 and $Cr(OH)_3$).[21,23,31–33]

The relatively large *FWHM* of oxidized Fe indicates that the spectra include several states of Fe(II) or Fe(III)-oxide, Fe(III)-oxyhydroxide, and Fe(III)-hydroxide. Although many authors have deconvoluted the oxidized Fe spectra into several peaks corresponding to the individual chemical states,[1–3,21,23–26] we treated the oxidized Fe as a single chemical state because the peak positions of the reported individual compounds differed between publications.[21,23–26,33,34] In the deconvolution, the peak energies were assumed to be constant for the quantitative analysis and the deconvolution process was very likely to introduce artificial error because of the selection of the peak positions. In this study we emphasized the quantitative ratio of the metal ions in the oxide rather than the detailed states of individual metallic ions. Thus, we estimated the relative intensities of the XPS peaks for the metal oxide from the assumption that it consists of a single state with a relatively large *FWHM*. For Ni, because the XPS signal of the Ni ion in the oxide was much weaker than that of the metallic element, we could not simulate the signal shape in detail. We assumed that the Ni ions were Ni^{2+} in NiO.[33] For Cr oxide, we estimated the relative intensity to be one compound (Cr-oxide) containing both Cr_2O_3 and $Cr(OH)_3$. From the relative intensity of the three metallic cations, quantitative analysis was performed to estimate the molar ratio of each ionic element (i.e., Fe, Cr, and Ni) in the passive oxide. The calibration of the concentration ratio of the metallic cations was achieved using the relative intensity of the XPS spectra corresponding to the metallic elements from the SS substrate. To estimate the relative intensity among the three metals, the spectra of the polished SS were recorded after Ar ion sputtering for 10 and 30 min at which the oxygen signal completely disappeared. After 10 min of sputtering, the intensities of the three metals changed very little. The relative intensities (I_{Fe}, I_{Cr},

Table I. Peak position (P_{BE}) and half width at half maximum (*FWHM*) of Fe2p3/2, Cr2p3/2, Ni2p3/2, and O1s for the calculation of intensities.

	Fe2p3/2		Cr2p3/2			Ni2p3/2		O1s		
	Fe(metal)	Fe-oxide	Cr(metal)	$Cr(OH)_3$	Cr_2O_3	Ni(metal)	NiO	O^{2-}	OH^-	H_2O
P_{BE}/eV	706.9 ± 0.1	709.5 ± 0.3	574.2 ± 0.1	577.4 ± 0.1	576.4 ± 0.1	852.8 ± 0.1	853.6 ± 0.2	530.2 ± 0.1	5301.8 ± 0.1	533.2 ± 0.2
FWHM/eV	2.0	4.0	2.2	3.8	2.2	1.4	2.2	1.6	1.8	1.8

Downloaded on 2016-06-13 to IP 133.87.145.210 address. Redistribution subject to ECS terms of use (see ecsdl.org/site/terms_use) unless CC License in place (see abstract).

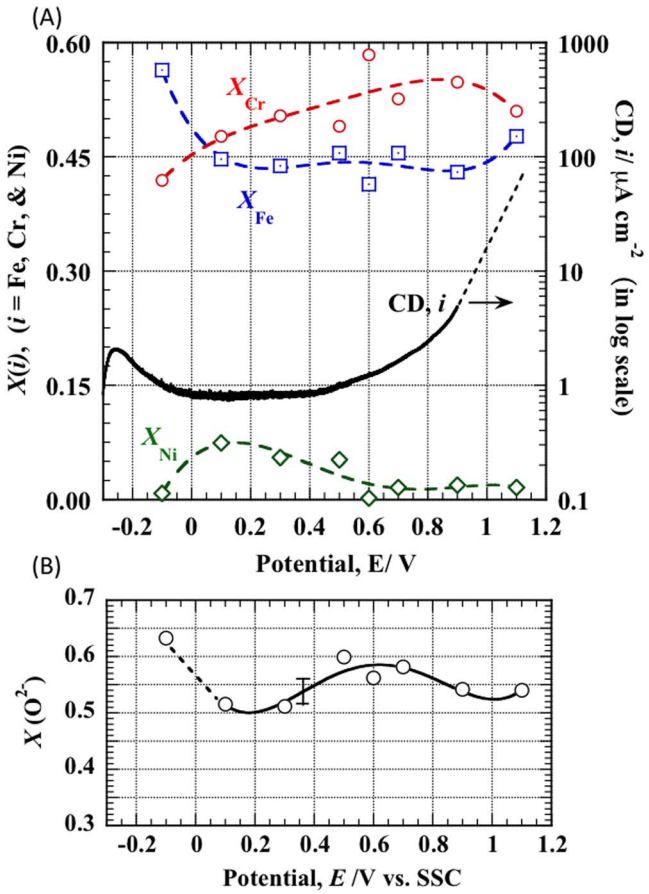

Figure 4. (A) Molar ratios of the Fe, Cr, and Ni cations and (B) molar ratio of O^{2-} to (O^{2-} + OH^-) in the passive oxide formed on SUS304 SS at various potentials in a 0.1 M H_2SO_4 solution. In Fig. (A), the log of CD as a function of potential was plotted with the data reported in Fig. 1.

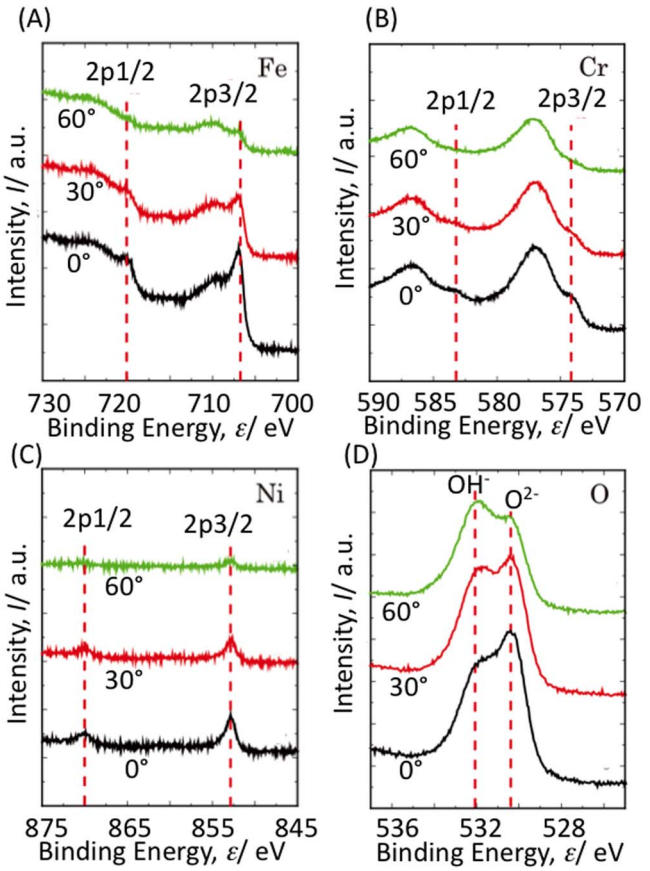

Figure 5. XPS spectra of (A) Fe, (B) Cr, (C) Ni, and (D) O of the passive oxide on SUS304 SS formed at 0.1 V vs. SSC for 1 h as a function of detection angle.

and I_{Ni}) of the XPS peaks of the three metals from the SS substrate after 10 min of sputtering were compared with the real molar ratios (x_{Fe}, x_{Cr}, and x_{Ni}) of the substrate:

$$a_{Fe} I_{Fe} : a_{Cr} I_{Cr} : a_{Ni} I_{Ni} = x_{Fe} : x_{Cr} : x_{Ni} \quad [4]$$

The calibration factors (a_{Fe}, a_{Cr}, and a_{Ni}) were then determined. The factors were used to determine the ratios of the three cations (i.e., Cr, Fe, and Ni ions) in the oxide film in the following section.

The molar ratios of the three cations in the passive oxide are shown in Fig. 4A as a function of potential. The Cr ratio was 0.47 at 0.1 V and gradually increased with potential to 0.58 at 0.6 V. At higher potentials in the transpassive region at 1.1 V, the Cr ratio decreased because of Cr(VI) dissolution. The Ni ratio was approximately 0.07 at 0.1 V, and this ratio decrease to 0.02 as the potential increased to more than 0.6 V. On the passive oxide formed on an Fe-18Cr-13Ni single crystal at 0.5 V vs. SHE for 2 h in a 0.5 M H_2SO_4 solution, Maurice et al.[3] reported the results from a simulation that Cr oxide was enriched at 62 mol% with the assumption of a bi-layer model consisting of an outer Cr-hydroxide layer and an inner Fe-Cr oxide layer. They also reported that Cr oxide was enriched at 55 mol% in the passive oxide formed on an Fe-17Cr single crystal at 0.39 V vs. SHE for 1 h in a 0.02 M NaCl solution[26] and at 90 mol% in the passive oxide on an Fe-22Cr single oxide at 0.50 V vs. SHE for 2 h in a 0.5 M H_2SO_4 solution.[24] The Cr enrichment in the passive oxide film was also reported on Fe-Cr alloys in an acidic H_2SO_4 solution by Asami et al.[21] and Kirchheim et al.[23] For the Fe-18Cr alloy, they found 62–65 mol% enrichment of Cr oxide in the passive oxide. The enrichment of Cr in the present study appears to be slightly smaller than that in the XPS results reported by these other authors.[21,23] Nevertheless, because the present results were estimated from the apparent intensities without any model simulation, the small difference from the molar fraction of Cr calculated from the model simulation by the other authors is reasonable.

In Fig. 4B, the ratio of O^{2-} to total oxygen (i.e., O^{2-} + OH^-) in the passive oxide was plotted as a function of potential. Because the intensity of the H_2O spectrum in the oxide was relatively small, its contribution was omitted. The molar ratio of O^{2-} reached 0.57 in a passive potential region of 0.5–0.7 V. In the initial passive and transpassive regions, the ratio was about 0.5.

The elemental profile as a function of depth was estimated by multiple-angle detection where the photoelectrons were detected as a function of the angle (θ) between the spectroscopic analyzer of the photoelectron and the normal to the specimen surface. The analytical depth, which is estimated by a distance in the perpendicular direction to the surface, was proportional to cos θ:

$$D(\theta) = D_0 \cos\theta \quad [5]$$

where D(θ) is the analytical depth measured at the angle θ and D_0 is the mean free path of a photoelectron with a given energy in the solid phase. From Eq. 5, the analytical depth is smaller with larger angles, and therefore, the molar ratios estimated from the XPS signals at larger angles represent the ratios in the outer portion of the passive oxide.[3,24]

The results by the multiple-angle detection are given in Fig. 5. Here, the XPS spectra of the SS passivated at 0.1 V for 3.6 ks were measured at three detection angles (i.e., 0, 30, and 60 deg). In Figs. 5A, 5B, and 5C, the peak intensities of the metallic elements in the substrate, denoted by the dashed lines, are seen to decrease at larger angles. This occurs because the signals from the metallic elements in the substrate are attenuated more in the oxide film by a smaller analytical depth at larger angles, according to Eq. 5. In Fig. 5D, the

Downloaded on 2016-06-13 to IP 133.87.145.210 address. Redistribution subject to ECS terms of use (see ecsdl.org/site/terms_use) unless CC License in place (see abstract).

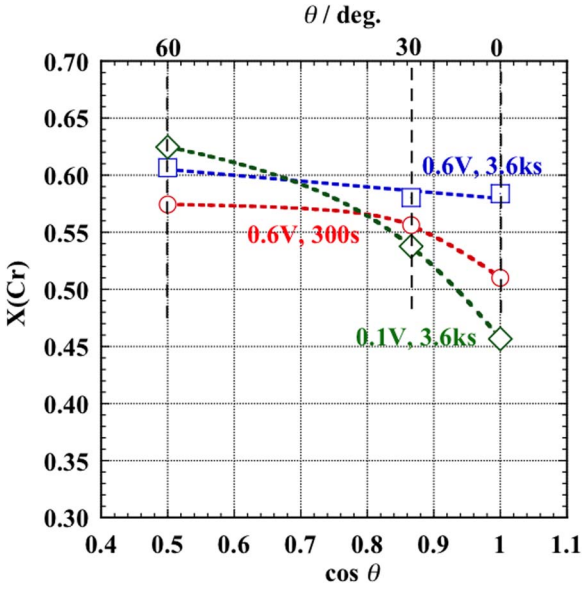

Figure 6. Dependence of the Cr ratio on the angle of detection (θ) of photoelectrons for the passive oxide formed on SUS304 SS at 0.1 V for 3.6 ks, at 0.6 V for 300 s, and at 0.6 V for 3.6 ks in 0.1 M H_2SO_4 solutions.

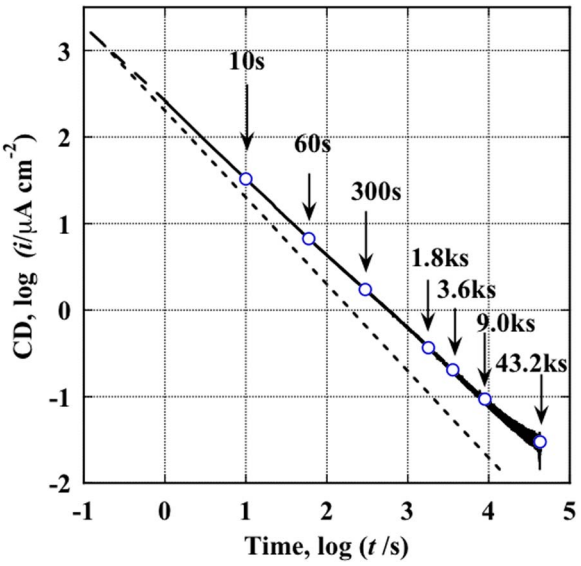

Figure 7. Decay of the current density under constant potential control at 0.6 V vs. SSC in a 0.1 M H_2SO_4 solution. The dashed line indicates the d(log *i*)/d(log *t*) = –1 relationship.

OH^- signal relative to the O^{2-} signal increased with a larger detection angle, indicating that OH^- preferentially distributes to the outer portion of the oxide film and O^{2-} mainly exists in the inner portion.

Figure 6 shows the average molar ratio of Cr in the passive oxide estimated at three detection angles (θ) as a function of cosθ. From the increase in the Cr ratio with a smaller cosθ, it is found that more Cr enrichment occurs at the outer portion of the passive oxide. Because greater distribution of OH^- was observed at the more outer portion in Fig. 5D, it is concluded that the outer oxide film contains more Cr hydroxide and the inner oxide film contains more Cr and Fe oxide.[3,24,26]

When one compares the X(Cr) at 0.6 V for 3.6 ks with that at 0.6 V for 300 s, the Cr oxide enriched at the outer portion in the initial 300 s spreads to the inner portion over time. When one compares the X(Cr) at 0.6 V for 3.6 ks with that at 0.1 V, the Cr enrichment is found to penetrate more readily into the inner part at 0.6 V than that at 0.1 V. It is assumed that Cr enrichment progresses in the whole oxide film under longer oxidation and higher potential.

The dependence of the XPS signals on the detection angle indicates that the Cr and OH- ions preferentially distribute into the outer portion of the passive oxide. From similar results, some authors assumed a two-layer structure in which the outer layer consists of Cr hydroxide and the inner layer consists of Cr and Fe oxides.[1,3,24–26] We question whether the thin oxide film at a 1–1.3 nm thickness (Fig. 1) can be divided into two layers.

Aging of the passive oxide during constant potential oxidation.— The CD decays with time at a constant potential in the passive region. Figure 7 shows the CD decay as a function of time on a logarithmic scale to 43.2 ks (12 h) during a potentiostatic oxidation at 0.6 V vs. SSC. The CD decreased with time from 1 mA cm^{-2} at 0.1 s to 0.02 μA cm^{-2} at 43.2 ks with a ratio of d[log(*i*)]/ d[log (*t*)] = –0.87. If one assumes that the CD is consumed without dissolution of the metallic cations in the formation of the passive oxide, which acts as a barrier against ionic migration under a high electric field, the ratio should become d[log(*i*)]/d[log (*t*)] = –1.[30] The smaller decay ratio in Fig. 7 indicates that the CD is partially consumed in the dissolution of the cations at the oxide/solution interface.[30]

The composition of the passive oxide was investigated during potentiostatic oxidation at 0.6 V using ex-situ XPS during the oxidation from 10 s to 43.2 ks by a similar manner as shown in Figs. 2–4. In Fig. 8A, the cationic ratios of Fe, Cr, and Ni in the passive oxide are plotted as a function of the time period at constant oxidation of 0.6 V, and in Fig. 8B, the ratio of O^{2-} to total oxygen (O^{2-} + OH^-) is plotted. The initial points in Figs. 8A and 8B indicate that the molar ratios in the air-formed oxide formed after polishing. In the air-formed oxide, Cr was already enriched.[23,36] Because the polishing was conducted on a buff moistened by an aqueous solution containing fine alumina powder, Fe and Ni was most likely preferentially dissolved during the polishing step, resulting in Cr enrichment to a molar ratio of 0.43 in the air-formed oxide film.[36] After reduction of the SS covered by the air-formed oxide at –0.4 V, Cr enrichment again occurs during potentiostatic oxidation at 0.6 V to a ratio of 0.57 in 10 ks. Kirchheim et al. also reported the gradual enrichment of Cr during the potentiostatic oxidation of Fe-18Cr alloys.[23] The cationic ratio of Fe, which had a molar ratio of 0.55 on the polished surface, decreased over time to approximately 0.4. The Ni ratio in the passive oxide was maintained at approximately 0.05. As shown in Fig. 8B, the O^{2-} ratio in the oxide increased from an initial value of 0.46 to 0.6 in 1 ks and then remained constant. Maurice et al. reported a similar gradual increase of O^{2-} in the Fe-22Cr alloy oxide with oxidation time.[24]

The change in the oxide thickness during potentiostatic oxidation at 0.6 V was measured by in-situ ellipsometry. Figure 9 shows the change in the ellipsometric parameters (i.e., Ψ and Δ) during the initial 600 s (10 min) oxidation (Fig. 9A) and the subsequent oxidation from 10 min to 13 h (Fig. 9B). The parameters were scattered in a range of (Ψ ± 0.015) deg. and (Δ ± 0.05) deg. The Δ value initially changes from 144.04 deg. for the reduced surface to 142.46 deg. at 10 s and then remained nearly constant at 142.45 deg. until 50 ks. The Ψ value initially decreased from 33.725 deg. to 33.675 deg. in 10 s and then decreased to 33.64 deg. in 3.6 ks. The subsequent change is small and the Ψ value became 33.66 deg. in 50 ks. Simultaneously, the reflectance change was measured, but the reflectance results were not used for the calculation of the film thickness in this study. The reflectance changed to $\Delta R/R_0 = -0.0076$ during the initial 5 s and then gradually changed to −0.043 in 43.2 ks (12 h). However, the Ψ and Δ values remained nearly constant except during the initial oxidation. We believe that the gradual decrease in the reflectance is caused by a small change in the roughness of the surface. We assume that the reflectance is sensitive to roughness, but Ψ and Δ are little influenced by the roughness and instead respond directly to the thickness change of the passive oxide.

Downloaded on 2016-06-13 to IP 133.87.145.210 address. Redistribution subject to ECS terms of use (see ecsdl.org/site/terms_use) unless CC License in place (see abstract).

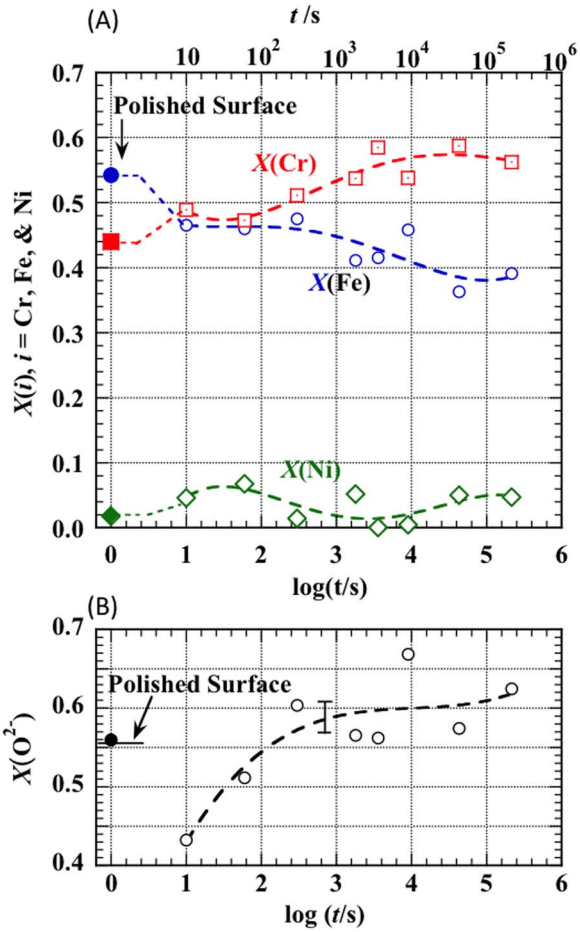

Figure 8. (A) Molar ratios of the Fe, Cr, and Ni cations and (B) molar ratio of O^{2-} to (O^{2-} + OH^-) in the passive oxide formed at 0.6 V in 0.1 M H_2SO_4 solution for various polarization times from 10 s to 43.2 ks. The solid marks on the left side indicate the molar ratios in the air-formed oxide on the mirror-like surface polished prior to passivation.

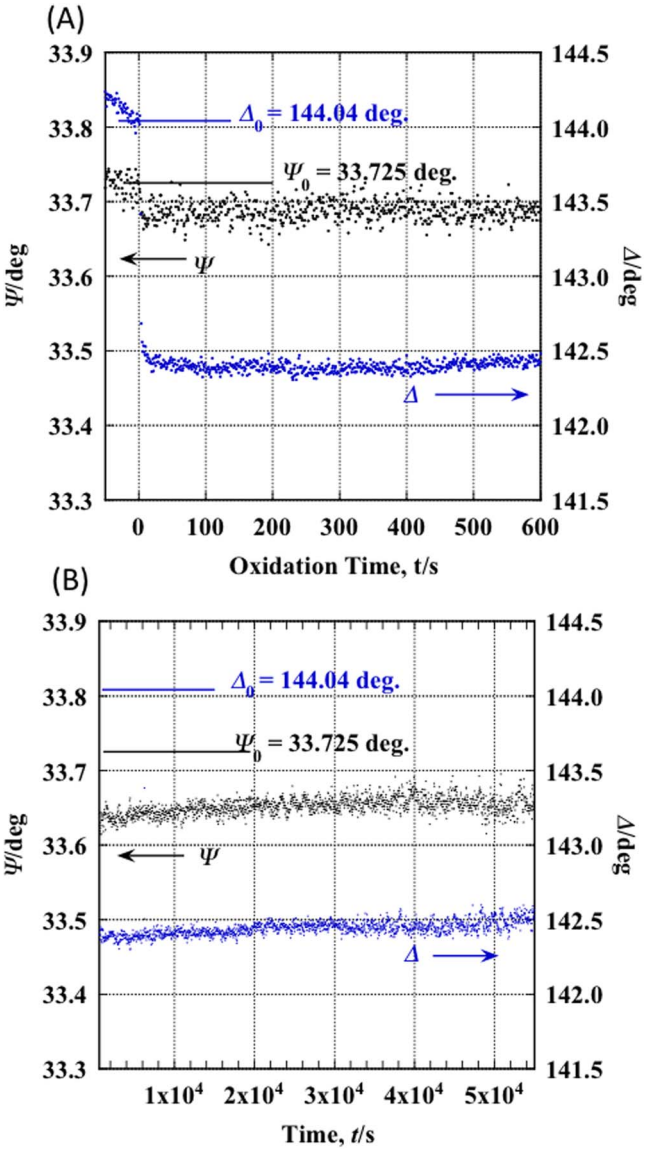

Figure 9. Change in Ψ and Δ from the initial values at $\Psi_0 = 33.725$ deg. and $\Delta_0 = 144.04$ deg. during the oxidation time at a constant potential of 0.6 V, (A) the initial period to 600 s (10 min), and (B) the period from 600 s to 55 ks (15.3 h).

The film thickness was estimated from the change in Ψ and Δ without using the reflectance change, which is influenced by both the surface roughness and oxide growth. For this estimate, we first calculated the complex refractive index N_s of the bare surface of the 304 SS from the values of the reduced surface: $\Psi_0 = 33.725$ deg. and $\Delta_0 = 144.04$ deg. The complex refractive index calculated was $N_3 = 3.1282 - j4.2143$ with the incidence angle at $\phi_1 = 60.0$ deg. and the refractive index of a 0.1 M H_2SO_4 solution at $n_1 = 1.340$. By using the above constants (n_1, N_3, and ϕ_1), we calculated the thickness of the oxide film from Ψ and Δ during the oxidation. The results are shown in Fig. 10. For the calculation we assumed a constant refractive index (from the real part of the complex refractive index, $N_2 = n_2 - jk_2$) for the passive oxide (i.e., $n_2 = 2.0$),[20] and from the change in Ψ and Δ, we estimated the extinction index (from the imaginary part of $N_2 = n_2 - jk_2$) and thickness (d). From the scattering of the measurement parameters at (Ψ ± 0.015) deg. and (Δ ± 0.05) deg., it is expected that the thickness can be calculated in a range of ± 0.05 nm. Figure 10 shows the estimated thickness (d) and extinction index (k_2) for the passive oxide during the initial oxidation for 600 s and the subsequent oxidation to 50 ks (13.9 h). The thickness of the passive oxide grows to 1.38 nm in the initial 300 s, decreases to 1.29 nm, and finally becomes constant at approximately 1.3 nm. Although Cr enrichment in the passive oxide occurs gradually during the long-term oxidation at 0.6 V, the thickness does not increase except during the initial 10 s and remains nearly constant at 1.3 nm.

The film thickness on the passive oxide has been estimated by XPS from the ratio of the signal intensity of the metallic elements in the substrate to the intensity of the ionic elements in the oxide, with the assumption of a mean free path or penetration distance of the photoelectrons.[3,21,24,34] Figure 11 shows the intensity ratios of the metallic to the ionic components of Fe and Cr as a function of the passivation time at 0.6 V. In Fig. 11, the decrease of the relative intensity of the metallic Fe and Cr over time is observed. In the oxide, if the mean free paths of individual photoelectrons from the metallic elements of Fe and Cr in the substrate were constant, the decrease of the relative intensity of the metallic elements would indicate a gradual increase of the thickness of the oxide film with time. However, this outcome disagrees with the ellipsometric results shown in Figs. 9 and 10. Because the oxide film is assumed to be denser with time since the O^{2-} component increases relative to OH^- (Fig. 8B) and more Cr-enriched oxide is produced (Fig. 8A), the mean free path in the oxide is not constant, but it may be expected to be shorter. We believe that the small growth in thickness of the oxide film with time on the basis

Downloaded on 2016-06-13 to IP 133.87.145.210 address. Redistribution subject to ECS terms of use (see ecsdl.org/site/terms_use) unless CC License in place (see abstract).

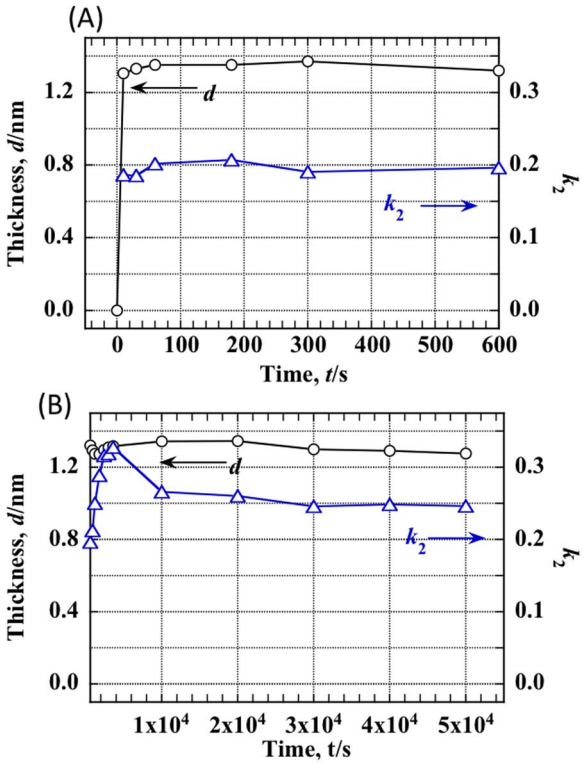

Figure 10. Film thickness of the passive oxide (d) as a function of oxidation time (t) at a constant potential at 0.6 V (A) for the initial period to 600 s (10 min), and (B) the period from 600 s to 50 ks (13.9 h).

of ellipsometry is not contradictory to the results in Fig. 11 from the XPS measurements.

The thickness was also estimated from a depth profile of each element by Ar^+ ion sputtering with an assumption of sputter efficiency.[24,33] In this study we did not use sputtering for the depth profile because this technique may induce a change of the oxidized states of the elements and oxygen state (O^{2-} or OH^-).

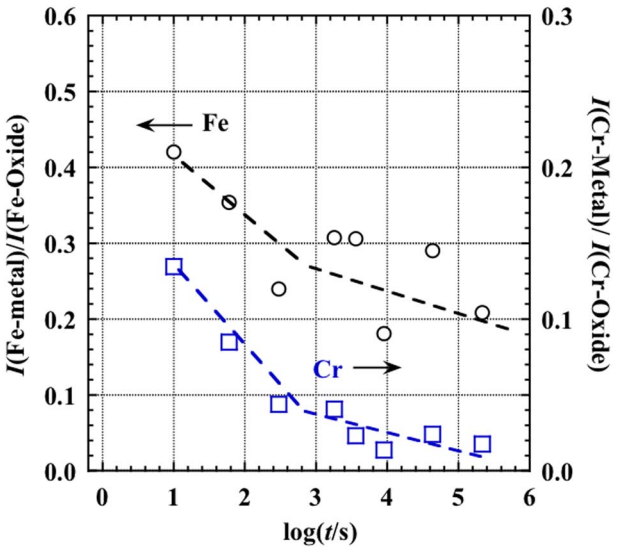

Figure 11. Intensity of the XPS peak of Fe(0) and Cr(0) relative to those of Fe(oxide) and Cr(oxide), respectively, as a function of time.

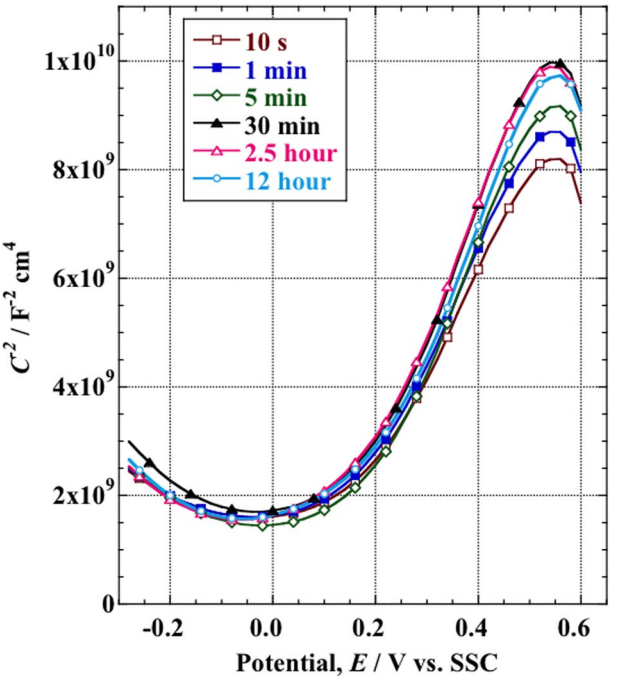

Figure 12. Mott-Schottky plot of the capacitance data on the passivated SUS304 SS at 0.6 V vs. SSC for 10 s, 60 s, 300 s, 9 ks, and 43.2 ks in a 0.1 M H_2SO_4 solution.

Semiconducting properties during aging under potentiostatic oxidation.—Cr was gradually enriched in the passive oxide during oxidation under constant potential control at 0.6 V. However, the thickness of the passive oxide remains nearly constant at 1.3 nm. The enrichment of Cr can be expected to influence the semiconducting properties of the passive oxide. To estimate the semiconducting properties, the Mott-Schottky relationship (Eq. 6)[5,6,10,20] was measured for the passive oxide formed at 0.6 V for 10 s to 4.32 ks.

$$C_{sp}{}^{-2} = (2/\varepsilon\varepsilon_0 N_D e)(E - E_{FB} - kT/e) \quad [6]$$

where C_{sp} is the space charge capacitance, N_D is the donor density, ε is the dielectric constant, ε_0 is the vacuum permittivity, and E_{FB} is the flatband potential. The measured capacitance (C) consists of the space charge capacitance in the passive oxide and the electric double layer capacitance at the oxide/solution interface. In general, because the reciprocal of the electric double layer capacitance is assumed to be much smaller than the reciprocal of the space charge capacitance, the contribution from the electric double layer capacitance to the measured capacitance is much smaller than that from the space charge capacitance. Therefore, the measured capacitance is assumed to be approximately equal to the space charge capacitance. The C^{-2} vs. E relationship for the oxide films formed at 0.6 V for various time periods is shown in Fig. 12. Here, the impedance was measured at a frequency of $f = 13$ Hz with a step-wise potential decrease from 0.60 V at a step height of 0.02 V and a step width of 10 s. The capacitance was calculated from the imaginary part (Y) of the complex impedance ($Z = X + jY$).

$$C = 1/(-2\pi f Y) \quad [7]$$

C^{-2} initially increased with a decrease in potential from 0.60 V and exhibited a maximum at approximately 0.5 V. At potentials between 0.5 V and 0.2 V, a linear relationship was observed, and the positive slope indicates that the passive oxide is an n-type semiconductor. The donor density was calculated from the slope of (dC^{-2}/dE) in the linear region assuming that $\varepsilon = 15.6$.[20] The calculated donor density is shown in Fig. 13. During the aging process, the donor density decreased from 4.5×10^{20} cm^{-3} to 3.5×10^{20} cm^{-3} as the oxidation time increased

Downloaded on 2016-06-13 to IP 133.87.145.210 address. Redistribution subject to ECS terms of use (see ecsdl.org/site/terms_use) unless CC License in place (see abstract).

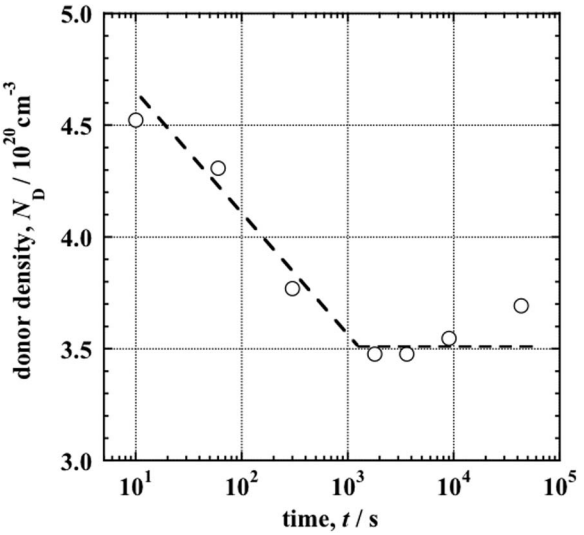

Figure 13. Donor density of the passive oxide film formed on SUS304 SS at 0.6 V vs. SSC for various times in a 0.1 M S_2SO_4 solution. The dielectric constant of the passive oxide was assumed to be 15.6.

from 10 s to 1.8 ks and then remained at 3.5×10^{20} cm^{-3} or slightly increased for time periods longer than 1.8 ks.

The change in the semiconducting property of the passive oxide as a function of oxidation time was further examined by measuring the redox current of Fe^{3+}/Fe^{2+} in a 0.1 M H_2SO_4 solution on the passive oxide.[37] Because electron transfer on the passivated SS is substantially influenced by the semiconducting property of the passive oxide, the redox current between Fe^{3+} and Fe^{2+} in a 0.1 M H_2SO_4 solution on the passivated SS was measured as a function of the oxidation time at 0.6 V.

$$Fe^{3+} + e^- \rightleftarrows Fe^{2+} \qquad [8]$$

Figure 14 shows the Fe^{3+}/Fe^{2+} redox current on a logarithmic scale measured as a function of the potential after passivation of the SS at 0.6 V for 3.6 ks. For comparison, the redox current on a Pt electrode is also plotted in Fig. 14. The CD was inhibited significantly on the

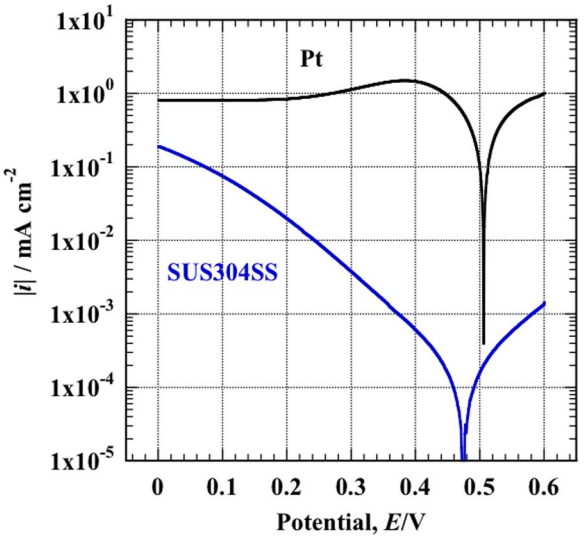

Figure 14. CD on a logarithmic scale as a function of the potential for the Fe^{3+}/Fe^{2+} redox reaction on SUS304 SS passivated at 0.6 V for 1 h in a 0.1 M H_2SO_4 solution. For comparison, the CD as a function of the potential on the Pt electrode was plotted. The sweep rate of the potential was 2 mV s^{-1}.

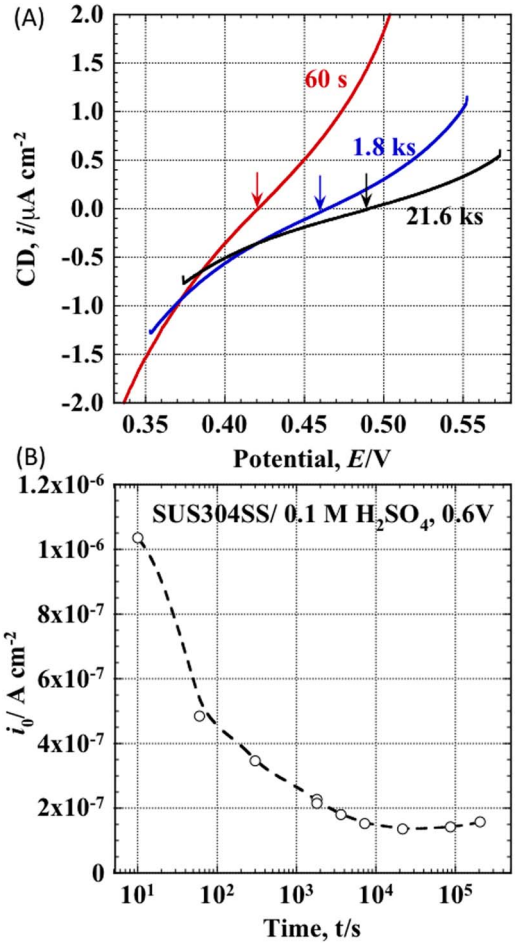

Figure 15. (A) CD as a function of the potential for the Fe^{3+}/Fe^{2+} redox reaction on 304 SS passivated at 0.6 V for 60 s, 1.8 ks, and 21.6 ks in a 0.1 M H_2SO_4 solution. (B) Exchange CD for the Fe^{3+}/Fe^{2+} redox reaction on 304 SS passivated at 0.6 V for various times.

passivated SS, and the zero-current potential ($E_{(i=0)}$) shifted to a more negative potential compared to that on the Pt electrode. Similar CD vs. potential curves were measured for various oxidation times. Examples of the CD-potential curves near the zero-current potential ($E_{(i=0)}$) are shown in Fig. 13A. With longer oxidation times, the slope of (di/dE) near $E_{(i=0)}$ becomes smaller. From the reciprocal of the polarization resistance, $R_p^{-1} = (di/dE)$, we estimated the exchange CD (i_0) of the redox reaction.

$$i_0 = 2.303^{-1} R_p^{-1}[(1/\beta_A) + (1/\beta_C)]^{-1} \qquad [9]$$

where β_A and β_C are the Tafel slopes of the anodic and cathodic currents, respectively, which were determined from the log $|i|$ vs. potential relationship shown in Fig. 14 for the SS passivated at 0.6 V for 3.6 ks. The exchange CD of the redox reaction thus calculated is plotted in Fig. 15B as a function of the oxidation time on a logarithmic scale. For 10 s of oxidation, the exchange CD is approximately 1.02 μA cm^{-2} and decreased to 0.15 μA cm^{-2} as the time increased to 10 ks. The results indicate that aging the passive oxide reduces the rate of the redox reaction to 1/8 compared to that in the initial 10 s of oxidation. During the aging process for long oxidation times, because Cr is enriched more in the oxide film without thickness growth, it is thus inferred that the Cr-enriched oxide film more effectively inhibits electron transfer from the SS substrate to the redox species in the electrolyte.

Downloaded on 2016-06-13 to IP 133.87.145.210 address. Redistribution subject to ECS terms of use (see ecsdl.org/site/terms_use) unless CC License in place (see abstract).

Discussion

Composition of the passive oxide.—Based on the XPS results on the passivated 304 SS shown in Fig. 4A, the passive film consists of 50–60% Cr oxide and 40–50% Fe oxide with a small amount of Ni oxide. The Cr oxide content in the passive oxide increased at higher potentials in the passive region but decreased in the transpassive region. The decrease in the transpassive region was caused by dissolution of CrO_4^{2-} ions. With the change in the Cr ratio, the ratio of O^{2-} to total oxygen increased at higher potentials in the passive region and decreased in the transpassive region, as shown in Fig. 4B. The Fe oxide component remained constant at approximately 44% in the passive region from 0.1 V to 0.9 V and increased at higher potentials in the transpassive region. The Ni content in the passive oxide is consistent with a molar ratio of approximately 0.07 at an initial passive potential of 0.1 V and becomes lower at higher potentials.

As shown in Fig. 8A, Cr enrichment was observed prior to anodic oxidation. The air-formed oxide film on the surface polished by an aqueous abrasive solution containing suspended alumina powder exhibited a molar ratio of Cr of approximately 0.44.[23,36] Following the removal of the air-formed oxide film by reduction at –0.4 V, the potentiostatic oxidation at 0.6 V again induced Cr enrichment to a molar ratio of 0.57 and depletion of Fe in the passive oxide. During aging at a constant potential of 0.6 V, enrichment of Cr and O^{2-} in the passive oxide gradually occurs. However, the oxide thickness remains 1.3 nm during oxidation from 10 s to 40 ks (Fig. 10). Although the thickness remains constant, the CD decays from 30 $\mu A\ cm^{-2}$ at 10 s to 0.025 $\mu A\ cm^{-2}$ at 43.2 ks (Fig. 6). The decay of CD was not caused by a thickening of the oxide but by enrichment of Cr and O^{2-}.

The dependence of the XPS signals on the detection angle, as shown in Figs. 5 and 6, indicates that the Cr and OH^- ions preferentially distribute to the outer portion of the passive oxide rather than the inner portion.

The composition of a typical passive oxide (e.g., the passive oxide at 0.6 V) can be described as follows. Under a quasi-stationary state after 10 ks of oxidation, the average ratios of the metal ions are 0.57 Cr, 0.40 Fe, and 0.03 Ni, and the molar ratios of the oxygen ion (O^{2-}) and hydroxide ion (OH^-) are 0.6 and 0.4, respectively. Cr and OH^- are distributed to the outer layer of the passive oxide at higher ratios than the average; in contrast, Fe and O^{2-} are distributed to the inner layer at higher ratios.

Enrichment of Cr in the passive oxide.—For the enrichment of Cr in the passive oxide, a relatively simple mechanism using a stationary state approximation can be considered. We assume two sets of ionic transfer reactions at the two respective interfaces.

The first process involves a mechanism that includes the preferential oxidation of Cr metal to Cr ion at the steel/oxide interface via the following interfacial reactions.

$$Fe\,(M) \rightarrow Fe^{2+\,or\,3+}\,(O) + (2\ or\ 3)\,e^-\,(M) \quad [10]$$

$$Cr\,(M) \rightarrow Cr^{3+}\,(O) + 3e^-\,(M) \quad [11]$$

$$Ni\,(M) \rightarrow Ni^{2+}\,(O) + 2e^-\,(M) \quad [12]$$

where (M) and (O) indicate the metal and oxide phase, respectively. Because Cr exhibits a lower equilibrium oxygen pressure at the metal/oxide interface than that of Fe and Ni, according to the well-known Ellingham diagram, Cr is likely to be preferentially oxidized at the interface.

The second process is the preferential dissolution of Fe and Ni ions at the oxide/solution interface via the following interfacial reactions.

$$Fe^{3+}\,(O) \rightarrow Fe^{3+}\,(S) \quad [13]$$

$$Cr^{3+}\,(O) \rightarrow Cr^{3+}\,(S) \quad [14]$$

$$Ni^{2+}\,(O) \rightarrow Ni^{2+}\,(S) \quad [15]$$

where (S) indicates the solution phase. The relation between the Cr enrichment and the preferential dissolution of Fe in Fe-Cr alloys was previously discussed by Kirchheim et al.[23] and Legrand et al.[25]

Regarding the origin of the Cr enrichment, we can further consider the different migration rates of the metal ions in the passive oxide.[23] When the migration rate of the Cr ion is relatively slower than that of the other metal ions, Cr should be enriched in the passive oxide, especially in the inner layer of the oxide. However, the simulation will become somewhat complicated when different migration rates are considered; thus, we disregard the contribution of migration rates. Next, we semi-quantitatively discuss the enrichment of Cr from the preferential oxidation at the steel/oxide interface and the preferential dissolution at the oxide/solution interface using a stationary state approximation.

We assume that the oxidation rates ($r_{i(M/O)}$) of Fe, Cr, and Ni at the metal/oxide interface are described by a product of the molar ratio ($X_{i(M)}$) of the steel substrate at the interface and the rate constant, which is independent of the composition of the substrate steel at the interface:

$$r_{i(M/O)} = k_{i(M/O)} X_{i(M)} \quad [16]$$

where i = Fe, Cr, or Ni and $k_{i(M/O)}$ is the rate constant for the i species in Reactions 10 to 12. In a similar fashion, we assume that the dissolution rates ($r_{i(O/S)}$) of Fe, Cr, and Ni at the oxide/solution interface are described by a product of the molar ratios ($X_{i(O)}$) of the oxide phase at the interface and the rate constant ($k_{i(O/S)}$), which is independent of the composition of the oxide:

$$r_{i(O/S)} = k_{i(O/S)} X_{i(O)} \quad [17]$$

The mutual relationship between $r_{i(M/O)}$ and $r_{i(O/S)}$ (i = Fe, Cr, and Ni) should provide the composition of the passive oxide. The change in the average molar ratio of the three metal cations (i.e., Fe, Cr, and Ni) in the oxide film can be described as follows:

$$(dX_{i(O)}/dt)d = r_{i(M/O)} - r_{i(O/S)} \quad [18]$$

where d is thickness of the oxide film. When one adopts the stationary state as a first approximation, the molar ratios in the oxide film are assumed to be constant and independent of time.

$$dX_{i(O)}/dt = 0 \quad [19]$$

From Eqs. 16–19, the molar ratio in the oxide film can be related to the ratio in the metal phase.

$$X_{i(O)} = (k_{i(M/O)}/k_{i(O/S)}) X_{i(M)} \quad [20]$$

From the experimental results for Cr enrichment ($X_{Cr(O)} > X_{Cr(M)}$) in the oxide film, the rate constant should be consistent with the following condition.

$$k_{Cr(M/O)} > k_{Cr(O/S)} \quad [21]$$

For Fe depletion, the rate constant should exhibit an inverse condition, that is,

$$(k_{Fe(M/O)} < k_{Fe(O/S)}) \quad [22]$$

For a more quantitative treatment, we conjecture that either of the two sets of ionic transfer reactions preferentially trigger Cr enrichment in the passive oxide. When the ionic transfer reaction at the metal/oxide interface controls the enrichment and no preferential dissolution occurs at the oxide/solution interface, the molar ratio in the dissolution reaction is directly proportional to the molar ratio of the oxide film, that is,

$$k_{Fe(O/S)} = k_{Cr(O/S)} = k_{Ni(O/S)} \quad [23]$$

From Eq. 20,

$$X_{Cr(O)} = (k_{Cr(M/O)}/k_{Fe(M/O)})(X_{Cr(M)}/X_{Fe(M)}) X_{Fe(O)} \quad [24]$$

Using the experimental results of $X_{Cr(O)} = 0.57$ and $X_{Fe(O)} = 0.40$ in Figs. 4 and 8A and the substrate composition of $X_{Cr(M)} = 0.18$ and $X_{Fe(M)} = 0.71$, the ratio of the reaction rate constants is

$$(k_{Cr(M/O)}/k_{Fe(M/O)}) = 5.6 \quad [25]$$

Downloaded on 2016-06-13 to IP 133.87.145.210 address. Redistribution subject to ECS terms of use (see ecsdl.org/site/terms_use) unless CC License in place (see abstract).

Thus, the oxidation rate of Cr is 5.6 times larger than that of Fe at the metal/oxide interface.

When the ionic transfer reaction at the oxide/solution interface preferentially controls the Cr enrichment (i.e., when the preferential dissolution of Fe and Ni occurs), the oxidation reaction rate of each metallic element at the metal/oxide interface is directly proportional to the molar ratio of the steel substrate.

$$k_{Fe(M/O)} = k_{Cr(M/O)} = k_{Ni(M/O)} \quad [26]$$

From Eq. 20,

$$X_{Cr(O)} = (k_{Fe(O/S)}/k_{Cr(O/S)})(X_{Cr(M)}/X_{Fe(M)})X_{Fe(O)} \quad [27]$$

Using a similar substitution of experimental results,

$$(k_{Cr(O/S)}/k_{Fe(O/S)}) = 0.18 \quad [28]$$

Thus, the dissolution rate of Cr is 5.6 times smaller than that of Fe at the oxide/solution interface. We cannot easily determine which of the two sets of ionic transfer reactions control Cr enrichment. If the difference in the oxidation rate constant of the metallic elements at the metal/oxide interface induces a change in composition, the enrichment of Cr in the passive oxide will be observed near the metal/oxide interface. If the difference in the dissolution rate constant at the oxide/solution interface induces a change in composition, the enrichment of Cr will be observed near the oxide/solution interface. Based on the multiple-angle-of-detection results of XPS shown in Figs. 5 and 6, Cr enriched occurs predominantly in the outer oxide layer. Therefore, the preferential dissolution at the oxide/solution interface is most likely the origin of Cr enrichment in the passive oxide. When Kirchheim et al.[23] assumed that the ratio of the rate constant of Fe dissolution to that of Cr dissolution at the oxide/solution interface was 500, which was evaluated from the stationary passive CDs of pure Fe and Cr in a sulfuric acid solution, they indicated that the Cr enrichment was over-estimated. They then assumed a difference in rate constants for the Fe and Cr ions in the ionic migration in the oxide film. When a ratio of the migration rate constant of Fe ions to that of Cr ion was assumed to be 8, the estimated Cr enrichment agreed with the experimental results. Because the rate constant of the ionic migration, for which they assumed to be a simple expression, can be replaced by the ratio of the dissolution rate constant,[23] the value of 5.6 determined in this study may not be considered too different from the value of 8 evaluated by Kirchheim et al. Additionally, Legrand et al. suggested a model for the Cr enrichment in the passive oxide on Fe-Cr alloys with the assumption of the selective dissolution of Fe.[25]

Relationship between Cr enrichment and the semiconducting properties.—During passivation at constant potential, the CD decayed with time and Cr was simultaneously enriched in the oxide film. In addition, the donor density of the oxide film decreased. The film thickness remained nearly constant at 1.3 nm from 10 s to 50 ks, even though the CD decreased 3 orders of magnitude from 30 μA cm^{-2} at 10 s to 0.025 μA cm^{-2} at 43.2 ks. If we assume that the CD is controlled by ionic migration caused by a high electric field, (dE/dx), in the oxide film, the decay of CD is accompanied by a gradual growth of the oxide thickness.[38,39]

$$i = i_0 \exp[(zae/kT)(dE/dx)] \quad [29]$$

where a is the half jump distance of the migrated species (or an activation distance), z is the valence of the migrating species, and i_0 is the migration CD at zero field. The electric field of dE/dx is replaced with an average electric filed ($\Delta E/d$) in the oxide film with a thickness (d):

$$i = i_0 \exp[(zae/kT)(\Delta E/d)] \quad [30]$$

where ΔE is the potential drop in the oxide film. If the composition and properties of the oxide film do not change with the aging time, i_0 and za remain constant. Therefore, a logarithm of CD (i) decays proportionally with (1/d) under constant potential control.

The results indicate that the film thickness was nearly constant and did not change with the aging time in which Cr was enriched relative to Fe and Ni. In addition, O^{2-} was enriched relative to OH^-. The gradual decay of CD was not induced by an increase in the thickness but by a change in the composition and properties of the oxide film (i.e., the change in the migration CD at zero field, i_0). The value of i_0 is assumed to be proportional to the density of mobile lattice defects (N_L) and a negative exponential of the activation energy ($\Delta G^{\#}$) for transfer between the stable lattice sites.

$$i_0 \approx N_L \exp(-\Delta G^{\#}/kT) \quad [31]$$

Therefore, the enrichment of Cr and O^{2-} in the oxide film during aging induces a decrease in mobile lattice defects and an increase in the activation energy. With the enrichment of Cr and O^{2-}, a more protective oxide film is formed that can sustain a potential drop in the oxide film caused by a smaller thickness.

The CD during the aging by constant potential oxidation at 0.6 V corresponds to a migration CD of ionic species or lattice defects in the oxide. However, the donor density in Fig. 13 and the exchange CD of the Fe^{3+}/Fe^{2+} redox couple in Fig. 15B are related to the defects in the electronic states. Although the relationship between the lattice and electronic defects should be examined in more detail, it can be suggested that both lattice and electronic state defects decrease with the enrichment of Cr and O^{2-} in the passive oxide during constant potential aging.

Conclusions

The passive oxide film on SUS 304 stainless steel (SS) was studied in a 0.1 mol dm^{-3} (M) sulfuric acid solution using ellipsometry, XPS, Mott-Schottky plots, and current measurements of the Fe^{3+}/Fe^{2+} redox couple.

(1) The Cr component was enriched to 57 mol% in the passive oxide film, and Cr and OH^- were more distributed in the outer portion of the oxide film than in the inner portion.
(2) During aging of the passive oxide at 0.6 V for 43 ks, the current decreased from 30 μA cm^{-2} at 10 s to 0.025 μA cm^{-2} at 43 ks and the Cr ratio in the passive oxide film simultaneously increased from 49 mol% to 57 mol%, which was accompanied by an increase in the O^{2-} ratio relative to OH^-. The film thickness remained nearly constant at 1.3 nm during the aging process.
(3) With the enrichment of Cr and O^{2-} in the passive oxide film during the aging, the donor density of the n-type semiconducting passive oxide decreased from 4.5×10^{20} cm^{-3} at 10 s to 3.5×10^{20} cm^{-3} at 2–43 ks, and the exchange current of the Fe^{3+}/Fe^{2+} redox reaction on the passive oxide decreased from 1.2 μA cm^{-2} at 10 s to 0.15 μA cm^{-2} at 22 ks.
(4) The possible origin of the Cr enrichment in the passive oxide film was discussed from a preferential dissolution of Fe and Ni relative to Cr.

References

1. S. Fujimoto, T. Yamada, and T. Shibata, *J. Electrochem. Soc.*, **145**, L79 (1998).
2. I. Olefjord, *Materials Sci. and Eng.*, **42**, 161 (1980).
3. V. Maurice, W. P. Yang, and P. Marcus, *J. Electrochem. Soc.*, **145**, 909 (1998).
4. G. Lorang, M. Da Cunha Belo, A. M. P. Simões, and M. G. S. Ferreira, *J. Electrochem. Soc.*, **141**, 3347 (1994).
5. N. E. Hakiki, M. Da Cunha Belo, A. M. P. Simões, and M. G. S. Ferreira, *J. Electrochem. Soc.*, **145**, 3821 (1998).
6. M. J. Carmezim, A. M. Simoes, M. F. Montemor, and M. da Cunha Belo, *Corros. Sci.*, **47**, 581 (2005).
7. S. Matsuda, K. Sugimoto, and Y. Sawada, *Transact. JIM*, **18**, 66 (1977).
8. K. Sugimoto and S. Matsuda, *Mater. Sci. Eng.*, **42**, 181 (1990).
9. S. V. Phadnis, M. K. Toniani, and D. Bhattachaya, *Transact. Inst. Metal. Finish.* **76**, 235 (1998).
10. A. Di Paola, *Electrochim. Acta*, **34**, 203 (1989).
11. A. M. P. Simoes, M. G. S. Ferreira, B. Rondot, and M. da Cunha Belo, *J. Electrochem. Soc.*, **137**, 82 (1990).
12. A. M. P. Simoes, M. G. S. Ferreira, B. Rondot, and M. da Cunha Belo, *Electrochim. Acta*, **36**, 315 (1991).
13. R. Babic and M. Metikos-Hukovic, *J. Electroanal. Chem.*, **358**, 143 (1993).

Downloaded on 2016-06-13 to IP 133.87.145.210 address. Redistribution subject to ECS terms of use (see ecsdl.org/site/terms_use) unless CC License in place (see abstract).

14. J.-P. Petit, A. Antoni, and B. Baroux, *European Federation of Corrosion Publication, No. 12*, *Modifications of passive films*, Ed. By P. Marcus, B. Baroux, and M. Keddam, The Institute of Metals (1994) 9.
15. T. L. Sudesh, L. Wijesinghe, and D. J. Blackwood, *Corros. Sci.*, **50**, 23 (2008).
16. A. Di Paola, D. Shukla, and U. Stimming, *Electrochim. Acta*, **36**, 345 (1991).
17. M. G. S. Ferreira, A. M. P. Simoes, C. Compere, B. Rondot, and M. da Cunha Belo, *Materials Sci. Forum*, **289-292**, 887 (1998).
18. M. G. S. Ferreira, N. E. Hakiki, G. Goodlet, S. Faty, A. M. P. Simões, and M. da Cunha Belo, *Electrochim. Acta*, **46**, 3767 (2001).
19. L. Freire, M. J. Carmezim, M. G. S. Ferreira, and M. F. Montemor, *Electrochim. Acta*, **55**, 6174 (2010).
20. T. Ohtsuka, Y. Sasaki, and A. Hyono, *Electrochim. Acta*, **60**, 384 (2012).
21. K. Asami, K. Hashimoto, and S. Shimodaira, *Corros. Sci.*, **18**, 151 (1978).
22. G. Hultquist, M. Seo, T. Leitbner, C. Leigraf, and N. Sato, *Corros. Sci.*, **27**, 937 (1987).
23. R. Kirchheim, B. Heine, H. Fischmesiter, S. Hofmann, H. Knote, and U. Stolz, *Corros. Sci.*, **29**, 899 (1989).
24. V. Maurice, W. P. Yang, and P. Marcus, *J. Electrochem. Soc.*, **143**, 1182 (1996).
25. M. Legrand, B. Diawara, J.-J. Legenfre, and P. Marcus, *Corros. Sci.*, **44**, 773 (2002).
26. W. P. Yang, D. Costa, and P. Marcus, *J. Electrochem. Soc.*, **141**, 111 (1994).
27. E. McCafferty, *Corros. Sci.*, **42**, 1993 (2000).
28. E. McCafferty, *Corros. Sci.*, **44**, 1393 (2002).
29. S. Qian, R. C. Newman, R. A. Cottis, and K. Sieradzki, *J. Electrochem. Soc.*, **137**, 435 (1990).
30. R. Kirchheim, *Electrochim. Acta*, **32**, 1619 (1987).
31. K. Asami and K. Hashimoto, *Corros. Sci.*, **17**, 559 (1977).
32. A. S. Lim and A. Atrens, *Appl. Phys.*, **A54**, 270 (1992).
33. S. Fujimoto, W.-S. Kim, M. Sato, J.-Y. Son, M. Machida, and H. Tsuchiya, *J. Sol. State Electrochem.*, **19**, 3521 (2015).
34. R.-H. Jung, Y. Tsuchiya, and S. Fujimoto, *Corros. Sci.*, **58**, 62 (2012).
35. C. Donic, A. Kocijan, D. Mandrino, and M. Jenko, *Metallurgy and Materials Transact. B*, **42**, 1044 (2011).
36. K. Asami and K. Hashimoto, *Corros. Sci.*, **45**, 2263 (2003).
37. T. Ohtsuka, M. Abe, and T. Ishii, *J. Electrochem. Soc.*, **162**, C528 (2015).
38. H. Cabrera and N. F. Mott, *Rep. Prog. Phys.*, **12**, 163 (1948).
39. N. F. Mott, *Trans. Faraday Soc.*, **43**, 429 (1947).

Downloaded on 2016-06-13 to IP **133.87.145.210** address. Redistribution subject to ECS terms of use (see **ecsdl.org/site/terms_use**) unless CC License in place (see abstract).